ICCEPM 2020
The 8th International Conference on Construction Engineering and Project Management
Dec. 7-8, 2020, Hong Kong SAR

Combining Machine Learning Techniques with Terrestrial Laser Scanning for Automatic Building Material Recognition

Liang Yuan[1], Jingjing Guo[2], Qian Wang[3*]

[1] *School of Management Science and Real Estate, Chongqing University, Chongqing, China 400045,* E-mail address: Yuanliang@cqu.edu.cn
[2] *Department of Building, School of Design and Environment, National University of Singapore, 4 Architecture Drive, Singapore 117566,* E-mail address: bdggj@nus.edu.sg
[3*] *Department of Building, School of Design and Environment, National University of Singapore, 4 Architecture Drive, Singapore 117566,* E-mail address: bdgwang@nus.edu.sg

Abstract: Automatic building material recognition has been a popular research interest over the past decade because it is useful for construction management and facility management. Currently, the extensively used methods for automatic material recognition are mainly based on 2D images. A terrestrial laser scanner (TLS) with a built-in camera can generate a set of coloured laser scan data that contains not only the visual features of building materials but also other attributes such as material reflectance and surface roughness. With more characteristics provided, laser scan data have the potential to improve the accuracy of building material recognition. Therefore, this research aims to develop a TLS-based building material recognition method by combining machine learning techniques. The developed method uses material reflectance, HSV colour values, and surface roughness as the features for material recognition. A database containing the laser scan data of common building materials was created and used for model training and validation with machine learning techniques. Different machine learning algorithms were compared, and the best algorithm showed an average recognition accuracy of 96.5%, which demonstrated the feasibility of the developed method.

Key words: Material recognition, Terrestrial laser scanner, Building material, Machine learning

1. INTRODUCTION

In the past decade, automatic building material recognition (a term used interchangeably with classification in the computer vision community) based on the state-of-the-art information technologies has been a promising research direction in the architecture, engineering, and construction (AEC) industry. Automatic material recognition can improve the efficiency of a variety of tasks, including damage detection and onsite material management and tracking [1,2]. Moreover, it has been an important task to generate as-is building information models (BIMs) that reflect the as-is conditions of facilities, which can be applied for various applications such as construction progress management, operation and maintenance (O&M) of existing buildings, and building performance analysis [3,4]. An as-is BIM, which can be applied for various applications such as construction progress management, operation and maintenance (O&M) of existing buildings, and building performance analysis [3,4], contains not only the geometric information of a building but also non-geometric information of building elements including building materials [5]. The material information is essential for many BIM applications such as building energy simulation and facility maintenance and repair. Therefore, there is a high demand for automatic building material recognition in order to generate semantically rich as-is BIMs containing material information.

Applying machine learning techniques for automatic building material recognition has been a popular approach over the past years. Currently, the proposed material recognition methods are mainly based on 2D images. The core technique of image-based methods focuses on using the visual features of building

materials such as colour, texture, roughness, and projection [3,6,7] for automatic recognition. However, image-based methods are heavily influenced by illumination conditions. Different illumination conditions strongly affect the visual characteristics of materials, causing difficulty for image-based building material recognition. Moreover, poor textures on objects and unknown viewpoints also negatively affect the robustness and accuracy of image-based material recognition [7].

Considering the potential of terrestrial laser scanning (TLS) for automatic building material recognition, this research aims to develop an automatic building material recognition approach based on TLS. A TLS with a built-in camera can capture not only the visual features but also intrinsic properties of building materials such as the material reflectance. Meanwhile, unlike passive imaging which is critically dependent on environmental lighting conditions, TLS uses an active measurement technique with infrared lights, which is not affected by environmental illumination conditions [8]. Therefore, TLS has great potentials to achieve more accurate material recognition considering the more types of information provided and higher robustness to changeable lighting conditions.

Moreover, TLS has been extensively adopted for as-is BIMs reconstruction due to its high measurement accuracy and speed [5]. As a result, using laser scan data for building material recognition does not require extra data collection if laser scan data are already collected for as-is BIMs reconstruction. Despite the advantages of TLS, few previous studies have adopted TLS for building material recognition.

2. RELATED WORKS

Image-based material recognition using computer vision techniques has been the dominant non-destructive material recognition method. Brilakis et al. [9,10] are among the first to introduce image-based material classification techniques into the construction industry, and their ground-breaking work validated the feasibility of image-based recognition of construction materials. After that, different image-based methods were increasingly developed for highly accurate, robust, and time-efficient material recognition for better construction management [3,6,7,11,12].

On the other hand, a few studies have explored building material classification based on TLS. The reflected intensity values collected by TLS are first adopted for material classification. For instance, Franceschi et al. [13] indicated that the intensity values from TLS could provide a reliable method to classify the rocks in outcrop conditions based on a series of experiments. Armesto González et al. [14] showed the potential of using the reflected intensity from TLS for the recognition and characterization of certain damages in building materials of historical buildings by combining digital image processing techniques and unsupervised classification algorithms. Riveiro et al. [15] presented a novel segmentation algorithm for automatic segmentation of masonry blocks from 3D laser scan data based on the reflected intensity values.

In addition to the reflected intensity values, some studies have utilized the colour information captured by the built-in camera of TLS for material classification. For example, Hassan et al. [16] confirmed the availability of material identification using the reflected intensity and Red-Green-Blue (RGB) values from TLS by a series of experiments. The experiment results showed that the scanned materials had different reflected intensity distributions, and the recorded RGB colour values could be used as a secondary parameter for material identification. Valero et al. [17] achieved automatic segmentation of individual masonry units and mortar regions in digitized rubble stone constructions based on coloured laser scan data acquired by TLS. The scan data of the target surface was converted into 2D depth maps as a feature for automatic segmentation, and colour information was used as another feature. The experimental results demonstrated the effectiveness of the technique.

Although image-based material recognition methods have made great advancement and are more extensively adopted than TLS-based methods, their applications in the real-world environment still face challenges due to the complex field conditions and their dependence on environmental illumination conditions. The ability to capture more types of information and the use of active measurement technique makes TLS-based material recognition more promising.

However, the previous studies on TLS-based material recognition are either based on only laboratory experiments in a controlled environment [13,14,16] or for the recognition of only one or two categories of building materials [15,17]. To tackle the limitations of previous studies, this study examines the feasibility of using TLS data for the recognition of ten different common building materials in real-world environments.

3. DETERMINATION AND CALCULATION OF FEATURES

In this study, the features used for automatic building material recognition are 1) material reflectance, 2) colour, and 3) surface roughness. For each scan point, the TLS collects a set of attributes comprising of the reflected laser beam intensity, RGB colour values, and x-y-z coordinates. The values of the chosen features can be calculated based on the collected information. The reasons for the determination of features and the calculation process of each feature are explained in the following subsections.

3.1. Material reflectance

For each scan point, the TLS provides a reflected laser intensity value (I_r), which is determined by the type of material and scanning parameters. Although I_r is recommended to be a feature for material classification in previous studies, different materials are likely to present similar I_r values because various scanning parameters can also affect I_r. Instead, among all the factors that affect I_r, the material reflectance ρ is the only intrinsic property of a certain material. In other words, the same material always has the same ρ value even though other factors are varying. Therefore, the material reflectance ρ is adopted as a feature for material recognition in this paper.

For calculating the ρ value from the TLS data, previous studies have proposed some methods [13,18], but these methods are not practical enough in the real-world environment because they require to place the same reference target in different scanning scenes to be a reference for the ρ calculation of the scanning target.

This study developed a reference target-free method for calculating the ρ values of different materials. Considering the realistic scanning scenes of buildings mostly being near-distance scanning, this study assumes that the scanning range R from the TLS to the scanned target is less than 10 m. For each laser scan point, the ρ value can be calculated for material recognition in the following three steps. First, the neighbouring points of a scan point are obtained by finding all points within a $s_1 \times s_1$ square that is centred at this scan point. As shown in Figure 1, all the points within the blue square become the neighbouring points of the blue point P_i. Second, the $\cos\theta/R^2$ values of the all neighbouring points are calculated by Equation (1) which is derived in the condition of long-distance scanning in previous studies [19-24]. Meanwhile, the I_r values of the neighbouring points are extracted from the laser scan data. Third, a linear function is fitted into the $\cos\theta/R^2$ and I_r values of neighbouring points according to Equation (2). This Equation is obtained based on a series of field tests using FARO Focus^{S}70 laser scanner in this study, and the coefficient ρK_1, ρK_2 or ρK_3 is obtained. Because ρK_1, ρK_2 or ρK_3 is fixed when using the same TLS and it is difficult to estimate their specific values, ρK_1, ρK_2 or ρK_3 is used in this study to represent ρ as the material reflectance for material recognition.

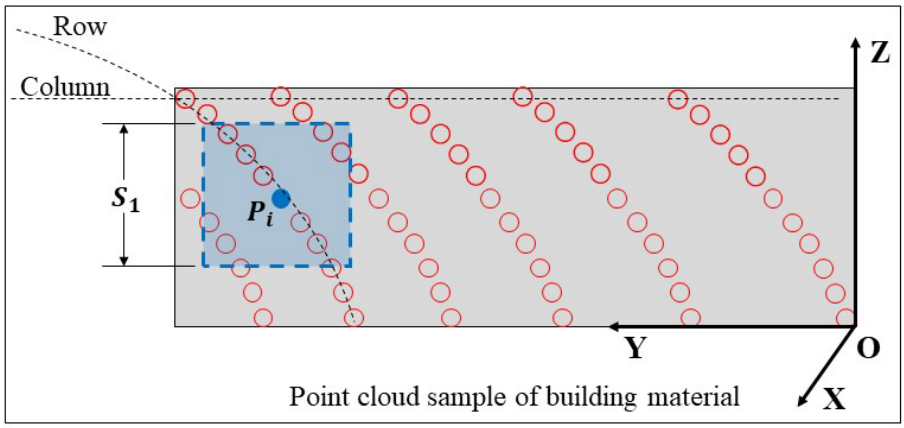

Figure 1. Calculation of ρ based on neighbouring points of a scan point

$$I_r = \rho K \frac{cos\theta}{R^2} = \rho K \frac{\sqrt{\frac{x^2+y^2}{x^2+y^2+z^2}}}{x^2+y^2+z^2} \quad (1)$$

where K is a total coefficient which comprises the transmitted intensity, the receiver aperture diameter, the atmospheric transmission factor, and the system transmission factor, and the K will be a fixed value

when using the same TLS for scanning. θ is the laser beam incident angle on I_r. x, y, z are the Cartesian coordinate values of each scanned point.

$$\left.\begin{aligned} I_r &= \rho K_1 \frac{cos\theta}{R^2} + b_1, \quad 4\,m < R < 10\,m \\ I_r &= \rho K_2 \frac{cos\theta}{R^2} + b_2, \quad 2\,m < R < 4\,m \\ I_r &= \rho K_3 \frac{\cos\theta}{R^2} + b_3, \quad R < 2\,m \end{aligned}\right\} \tag{2}$$

where b_1, b_2, and b_3 are three different constant terms. They exist because of the equipped brightness reducer in the scanner to protect the scanner from extremely high received laser intensity [24,25].

3.2. Colour

A TLS with a built-in camera can capture the colour information of each scan point and record as RGB colour space (RGB values from 0 to 255). The RGB values can potentially help in building material recognition. Object colours have been extensively used for not only object and material recognition using 2D images in the computer vision community [3-5,26], but also material classification using laser scan data [16,17]. According to the literature, the Hue-Saturation-Value (HSV) colour space is preferred than the RGB colour space because of its better robustness under variable illumination conditions. Therefore, this study also adopts the HSV colour space as the features for automatic building material recognition. The translation function from RGB to HSV is described in [27], as follows:

$$\left.\begin{aligned} r = \frac{R}{255}, g = \frac{G}{255}, b = \frac{B}{255} \\ Ma = max(r,g,b)\,, Mi = min(r,g,b), \Delta = Ma - Mi \\ H = \begin{cases} 0^o, & if\ Ma = Mi \\ 60^o \times \dfrac{g-b}{\Delta} + 0^o, & if\ Ma = r\ and\ g \gg b \\ 60^o \times \dfrac{g-b}{\Delta} + 360^o, & if\ Ma = r\ and\ g < b \\ 60^o \times \dfrac{b-r}{\Delta} + 120^o, & if\ Ma = g \\ 60^o \times \dfrac{r-g}{\Delta} + 240^o, & if\ Ma = b \end{cases} \\ S = \begin{cases} 0, & if\ Ma = 0 \\ \dfrac{\Delta}{Ma}, & otherwise \end{cases} \\ V = Ma \end{aligned}\right\} \tag{3}$$

3.3. Surface roughness

With the millimetre-level laser beam diameter, TLS can capture microscopic characteristics of building materials, e.g. surface roughness (R_a). The feasibility of estimating surface roughness based on laser scan data has been proven by previous research efforts [28,29]. In general, each category of building material presents different surface roughness. Previous studies show that it is potential to utilize surface roughness estimated from laser scan data for material recognition. Therefore, this research also uses surface roughness as a feature for automatic building material recognition.

In this study, the surface roughness R_a of a scan point is calculated in the following four steps. First, for each scan point P_i, its neighbouring points are obtained as the points within the $s_2 \times s_2$ square that is centred at this point, as shown in Figure 2. Second, a plane is fitted into the neighbouring points using the M-estimator SAmple Consensus (MSAC) algorithm. The fitted plane M can be expressed as $Ax + By + Cz + D = 0$. Third, the orthogonal distance d_i from each neighbouring point (x_i, y_i, z_i) to the fitted plane is calculated using Equation (4):

$$d_i = \frac{|Ax_i + By_i + Cz_i + D|}{\sqrt{A^2 + B^2 + C^2}} \tag{4}$$

Lastly, the surface roughness R_a at point P_i is calculated as the average d_i value for all the n neighbouring points:

$$R_a = \frac{1}{n}\sum_{i=1}^{n} d_i \tag{5}$$

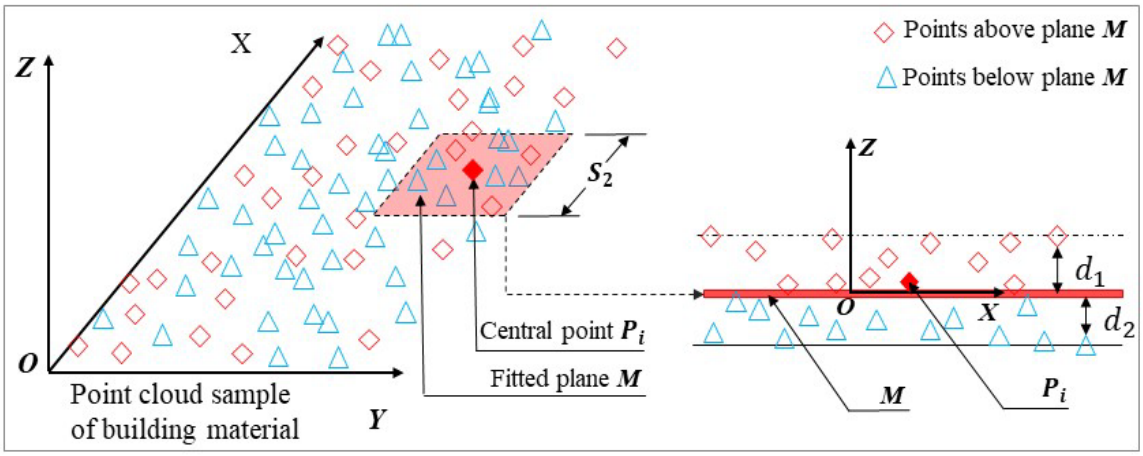

Figure 2. Calculation of surface roughness based on neighbouring points and fitted plane

4. EXPERIMENTS

Taking the existing construction material libraries as a reference, we created a common building material set. This study considered ten different categories of materials, including concrete, mortar, stone, metal, painting, wood, plaster, plastic, pottery, and ceramic. Although being extensively used in buildings, glass is not chosen in this study because TLS has difficulty in capturing transparent objects. For the ten categories of materials, one specific commonly-used building material was selected from each category.

A FARO Focus^{S}70 TLS was used to collect laser scan data of the ten materials. This TLS had a measurement range of 0.6 to 70 m, and a field of view of 300° vertically and 360° horizontally. The beam diameter was 2.12 mm, and the divergence was 0.3 mrad [30]. The laser scan data of the ten building materials were collected from buildings in the National University of Singapore. The collected scan data included both building interiors (i.e. ceilings, walls, and floors) and exterior facades. The data processing was executed in MATLAB2019a [31] after the laser scan data were extracted from the TLS's software FARO SCENE [32].

We created a dataset with $2\,m < R < 4m$ contained 41,000 data points (approximately 4,100 data points for each building material), and the dataset with $4\,m < R < 10\,m$ contained 53,000 data points (approximately 5,300 data points for each building material). This study did not choose $R < 2\,m$ because the scanning scenes with it are very rare in laser scanning of buildings. Each data point comprised a building material category label, ρ value, H, S, and V values in the HSV colour space, and R_a value. To find the best combination of features, this study tested different combinations of features (ρ, HSV values, and R_a). Besides, the I_r value and RGB values were also considered in the comparisons. To identify the best recognition model, different supervised learning classifiers were explored.

Recognition accuracy was used in this research to measure the performance of different recognition models. The accuracy of a recognition model can be quantified by Equation (6).

$$Accuracy = \frac{TP + TN}{TP + TN + FP + FN} \quad (6)$$

where *TP*, *TN*, *FP*, and *FN* are the numbers of True Positives, True Negatives, False Positives, and False Negatives, respectively.

4.1. Experiment Results

We trained different classifiers with different feature combinations in Classification Learner of MATLAB2019a. Two accuracy performance matrixes with different ranges of R are obtained, as shown in Tables 1 and 2.

Table 1. The accuracy performance matrix of building material recognition when $2\,m < R < 4\,m$

	DTs (%)	**Das (%)**	**NBs (%)**	**SVMs (%)**	**KNNs (%)**	**Ensembles (%)**
$\boldsymbol{\rho}$	61.0	54.7	59.0	60.3	61.8	58.6
$\boldsymbol{R_a}$	28.0	26.5	28.8	30.1	28.1	31.4
$\boldsymbol{HSV}$	85.7	73.4	78.5	82.7	88.1	88.6
$\boldsymbol{RGB}$	71.9	78.1	53.5	80.6	87.5	88.6
$\boldsymbol{I_r}$	40.3	38.8	40.4	38.9	35.4	40.2
$\boldsymbol{\rho + R_a}$	69.3	53.8	65.9	63.8	72.7	70.4
$\boldsymbol{\rho + HSV}$	89.0	86.2	89.1	88.1	94.2	95.0
$\boldsymbol{R_a + HSV}$	86.2	73.5	82.5	89.1	90.0	92.5
$\boldsymbol{\rho + R_a + HSV}$	91.0	88.7	91.2	93.1	95.2	**96.1**

Table 2. The accuracy performance matrix of building material recognition when $4\,m < R < 10\,m$

	DTs (%)	**Das (%)**	**NBs (%)**	**SVMs (%)**	**KNNs (%)**	**Ensembles (%)**
$\boldsymbol{\rho}$	77.0	67.6	74.9	72.0	77.5	75.7
$\boldsymbol{R_a}$	30.9	26.6	26.0	26.0	24.7	29.5
$\boldsymbol{HSV}$	71.5	67.1	71.9	72.2	75.0	77.7
$\boldsymbol{RGB}$	65.8	68.2	48.8	60.8	75.0	76.3
$\boldsymbol{I_r}$	29.7	24.6	24.6	24.5	28.5	29.4
$\boldsymbol{\rho + R_a}$	85.3	71.5	78.6	79.1	87.2	86.8
$\boldsymbol{\rho + HSV}$	93.5	88.9	91.2	90.8	95.6	95.9
$\boldsymbol{R_a + HSV}$	77.9	69.5	77.0	80.0	82.7	84.4
$\boldsymbol{\rho + R_a + HSV}$	94.1	89.6	95.2	90.5	96.6	**97.0**

According to Table 1, when $2\,m < R < 4\,m$, using ρ, HSV, and R_a as features and Ensemble as the classifier produced the highest recognition accuracy of 96.1%. According to Table 2, when $4\,m < R < 10\,m$, using ρ, HSV, and R_a as features and Ensemble as the classifier produced the highest recognition accuracy of 97.0%. In conclusion, using ρ, HSV, and R_a as features and Ensemble as the classifier always had the highest recognition accuracy, showing an average recognition accuracy of 96.5% when $2\,m < R < 10\,m$.

As mentioned above, this study used ρ instead of I_r, and HSV instead of RGB as the features for material recognition. The experiments also tested the recognition accuracy when using ρ, I_r, HSV, or RGB as the only feature. According to Tables 1-2, using ρ as the only feature had accuracies of 61.8%

and 77.5%, respectively, which were higher than the accuracies of 40.4% and 29.7% when using I_r. The experimental results showed that ρ was a much better feature for material recognition than I_r. For the comparisons between HSV and RGB, using HSV colours as the only features had accuracies of 88.6% and 77.7%, respectively. The accuracies became 88.6% and 76.3% when using RGB colours. Although the accuracies were very similar, HSV colours still had a better overall performance than RGB colours. The comparisons proved that selecting ρ and HSV colours as features was preferred.

We further compared the performances when using any two of ρ, HSV, and R_a as the features (i.e. $\rho + R_a$, $\rho + HSV$, and $R_a + HSV$). Tables 1-2 proved that using the combination of any two features performed better than using any single feature on recognition accuracy. The results indicated that all the features were useful for improving recognition accuracy.

Regarding the comparisons of classifiers, the experimental results showed that the ensemble algorithm was the best classifier. The result is consistent with the conclusion introduced in a previous study [26]. According to the experimental results, the algorithm with the highest recognition accuracy was the bootstrap-aggregated decision trees (Bagged Trees) in both Tables 1 and 2.

4.2. Discussion

To further understand the material recognition results, we used the confusion matrix to analyse the recognition performance for the case with the highest recognition accuracy (i.e. using $\rho + R_a + HSV$ as features and Bagged Trees algorithm as the classifier). The recognition results for both $2\ m < R < 4\ m$ and $4\ m < R < 10\ m$ were combined, and the confusion matrix is shown in Figure 3. Each row of the confusion matrix shows the percentage of *TP* and *FN* for a true material class. It is found that all ten categories of materials produced a recognition accuracy of at least 92%. The painting material showed the highest *TP* percentage of 100%, indicating that all the data of the painting material were correctly recognized. The mortar material presented the lowest recognition accuracy of 92%. It is shown that 7% of mortar data were wrongly recognized as stone. This phenomenon indicated that the features of stone material were similar to these of mortar material.

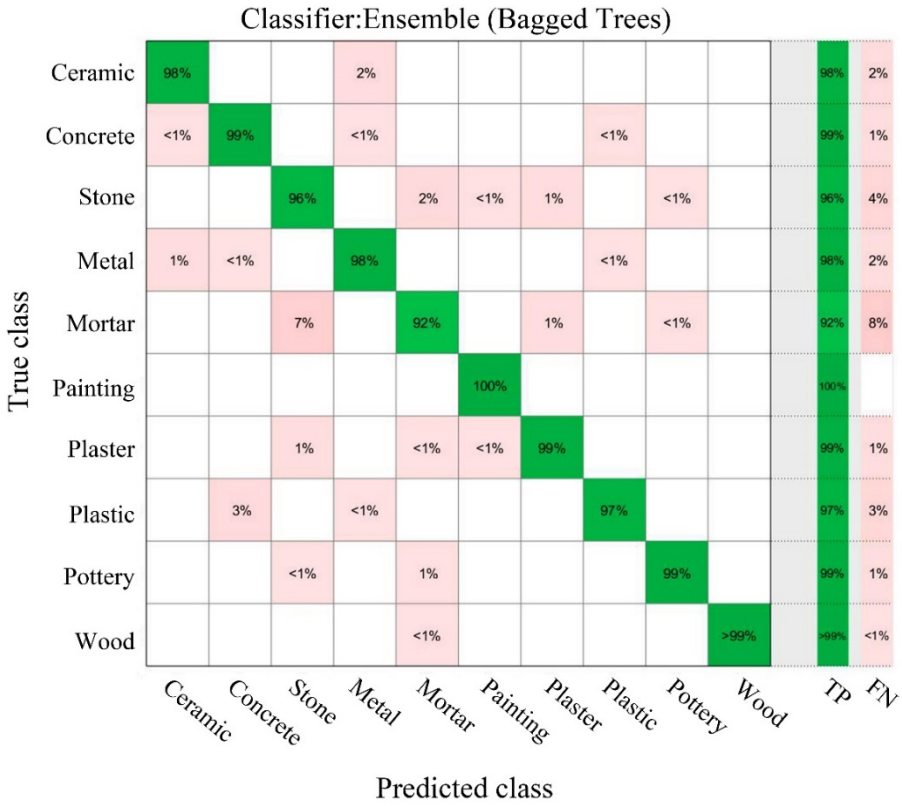

Figure 3. Confusion matrix of the case with the highest recognition accuracy (i.e. using $\rho + R_a + HSV$ as features and Bagged Trees algorithm as the classifier)

5. CONCLUSION

Automatic material recognition can improve the efficiency of a variety of tasks, including damage detection and onsite material management and tracking. Particularly, as BIM is popularly adopted in the

AEC industry, there is a high demand for automatic building material recognition in order to generate semantically rich as-is BIMs containing material information. While the previous studies are focused on material recognition methods based on 2D images, this study proposes to combine machine learning techniques into TLS for material recognition because TLS provides more types of information and has better robustness to lighting conditions.

In the proposed method, material reflectance ρ, HSV colours, and surface roughness R_a are used as recognition features. The ρ value is an intrinsic property of a certain material, and it can be inferred from the TLS data. The HSV colours are used in this study instead of the RGB colours because the HSV colours show better robustness to varying lighting conditions. The HSV colours are calculated from RGB colours that are obtained from the raw laser scan data. The R_a value is calculated as the average distance from the neighbouring points of a scan point to the fitted plane of the neighbouring points.

To validate the proposed method, we used different supervised learning classifiers to test the different combinations of features. Ten different categories of materials, including concrete, mortar, stone, metal, painting, wood, plaster, plastic, pottery, and ceramic, are selected as test samples. A FARO Focus^{S}70 TLS was used to collect laser scan data of the ten different materials. The laser scan data were processed in MATLAB2019a to calculate the above-mentioned features. In the model training and testing, we used 80% of the entire dataset to train the recognition model and the rest 20% to test the trained model. The experimental results showed that using ρ, HSV, and R_a as features and Ensemble as the classifier realized an average recognition accuracy of 96.5%. Experimental results also validated that ρ was a much better feature for material recognition than I_r, and HSV colour outperformed RGB colour. Further analyses showed that all the ten categories of materials produced a recognition accuracy of at least 92% when using $\rho + R_a + HSV$ as features and Bagged Trees algorithm as the classifier.

REFERENCES

[1] J. DeGol, M. Golparvar-Fard, D. Hoiem, "Geometry-informed material recognition", In Proceedings of the IEEE Conference on Computer Vision and Pattern Recognition, Las Vegas, NV, USA, pp. 1554-1562, 2016, https://doi.org/10.1109/cvpr.2016.172.

[2] J.E. Meroño, A.J. Perea, M.J. Aguilera, A.M. Laguna, "Recognition of materials and damage on historical buildings using digital image classification", South African Journal of Science, vol. 111, no. 1-2, pp. 1-9, 2015, https://doi.org/10.17159/sajs.2015/20140001.

[3] K.K. Han, M. Golparvar-Fard, "Appearance-based material classification for monitoring of operation-level construction progress using 4D BIM and site photologs", Automation in Construction, vol. 53, no. 44-57, 2015, https://doi.org/10.1016/j.autcon.2015.02.007.

[4] Q. Wang, M. Kim, "Applications of 3D point cloud data in the construction industry: A fifteen-year review from 2004 to 2018", Advanced Engineering Informatics, vol. 39, no. 306-319, 2019, https://doi.org/10.1016/j.aei.2019.02.007.

[5] Q. Lu, S. Lee, "Image-based technologies for constructing as-is building information models for existing buildings", Journal of Computing in Civil Engineering, vol. 31, no. 4, pp. 4017005, 2017, https://doi.org/10.1061/(asce)cp.1943-5487.0000652.

[6] H. Son, C. Kim, N. Hwang, C. Kim, Y. Kang, "Classification of major construction materials in construction environments using ensemble classifiers", Advanced Engineering Informatics, vol. 28, no. 1, pp. 1-10, 2014, https://doi.org/10.1016/j.aei.2013.10.001.

[7] Q. Lu, S. Lee, L. Chen, "Image-driven fuzzy-based system to construct as-is IFC BIM objects", Automation in Construction, vol. 92, no. 68-87, 2018, https://doi.org/10.1016/j.autcon.2018.03.034.

[8] S.Y. Chen, Y.F. Li, W. Wang, J. Zhang, "Active sensor planning for multiview vision tasks", Berlin Heidelberg: Springer, pp. 25-27, 2008, https://doi.org/10.1007/978-3-540-77072-5.

[9] I. Brilakis, L. Soibelman, Y. Shinagawa, "Material-based construction site image retrieval", Journal of Computing in Civil Engineering, vol. 19, no. 4, pp. 341-355, 2005, https://doi.org/10.1061/(asce)0887-3801(2005)19:4(341).

[10] I.K. Brilakis, L. Soibelman, Y. Shinagawa, "Construction site image retrieval based on material cluster recognition", Advanced Engineering Informatics, vol. 20, no. 4, pp. 443-452, 2006,

[11] A. Dimitrov, M. Golparvar-Fard, "Vision-based material recognition for automated monitoring of construction progress and generating building information modeling from unordered site image collections", Advanced Engineering Informatics, vol. 28, no. 1, pp. 37-49, 2014, https://doi.org/10.1016/j.aei.2013.11.002.

[12] Z. Zhu, I. Brilakis, "Parameter optimization for automated concrete detection in image data", Automation in Construction, vol. 19, no. 7, pp. 944-953, 2010, https://doi.org/10.1016/j.autcon.2010.06.008.
[13] M. Franceschi, G. Teza, N. Preto, A. Pesci, A. Galgaro, S. Girardi, "Discrimination between marls and limestones using intensity data from terrestrial laser scanner", Isprs Journal of Photogrammetry and Remote Sensing, vol. 64, no. 6, pp. 522-528, 2009, https://doi.org/10.1016/j.isprsjprs.2009.03.003.
[14] J. Armesto-González, B. Riveiro-Rodríguez, D. González-Aguilera, M.T. Rivas-Brea, "Terrestrial laser scanning intensity data applied to damage detection for historical buildings", Journal of Archaeological Science, vol. 37, no. 12, pp. 3037-3047, 2010, https://doi.org/10.1016/j.jas.2010.06.031.
[15] B. Riveiro, P.B. Lourenço, D.V. Oliveira, H. González Jorge, P. Arias, "Automatic morphologic analysis of quasi‐periodic masonry walls from LiDAR", Computer‐Aided Civil and Infrastructure Engineering, vol. 31, no. 4, pp. 305-319, 2016, https://doi.org/10.1111/mice.12145.
[16] M.U. Hassan, A. Akcamete-Gungor, C. Meral, “Investigation of Terrestrial Laser Scanning Reflectance Intensity and RGB Distributions to Assist Construction Material Identification”, Proceedings of the Joint Conference on Computing in Construction, Heriot-Watt University, 2017, https://doi.org/10.24928/jc3-2017/0312.
[17] E. Valero, F. Bosché, A. Forster, "Automatic segmentation of 3D point clouds of rubble masonry walls, and its application to building surveying, repair and maintenance", Automation in Construction, vol. 96, no. 29-39, 2018, https://doi.org/10.1016/j.autcon.2018.08.018.
[18] K. Tan, X. Cheng, "Surface reflectance retrieval from the intensity data of a terrestrial laser scanner", Journal of the Optical Society of America A, vol. 33, no. 4, pp. 771-778, 2016, https://doi.org/10.1364/josaa.33.000771.
[19] B. Höfle, N. Pfeifer, "Correction of laser scanning intensity data: Data and model-driven approaches", Isprs Journal of Photogrammetry and Remote Sensing, vol. 62, no. 6, pp. 415-433, 2007, https://doi.org/10.1016/j.isprsjprs.2007.05.008.
[20] C. Suchocki, J. Katzer, "Terrestrial laser scanning harnessed for moisture detection in building materials–Problems and limitations", Automation in Construction, vol. 94, no. 127-134, 2018, https://doi.org/10.1016/j.autcon.2018.06.010.
[21] S. Kaasalainen, A. Jaakkola, M. Kaasalainen, A. Krooks, A. Kukko, "Analysis of incidence angle and distance effects on terrestrial laser scanner intensity: Search for correction methods", Remote Sensing, vol. 3, no. 10, pp. 2207-2221, 2011, https://doi.org/10.3390/rs3102207.
[22] W. Fang, X. Huang, F. Zhang, D. Li, "Intensity correction of terrestrial laser scanning data by estimating laser transmission function", Ieee Transactions On Geoscience and Remote Sensing, vol. 53, no. 2, pp. 942-951, 2015, https://doi.org/10.1109/tgrs.2014.2330852.
[23] A. Krooks, S. Kaasalainen, T. Hakala, O. Nevalainen, "Correction of intensity incidence angle effect in terrestrial laser scanning", ISPRS Annals of Photogrammetry, Remote Sensing and Spatial Information Sciences, vol. 2, no. 145-150, 2013, https://doi.org/10.5194/isprsannals-ii-5-w2-145-2013.
[24] S. Kaasalainen, A. Krooks, A. Kukko, H. Kaartinen, "Radiometric calibration of terrestrial laser scanners with external reference targets", Remote Sensing, vol. 1, no. 3, pp. 144-158, 2009, https://doi.org/10.3390/rs1030144.
[25] S. Kaasalainen, A. Kukko, T. Lindroos, P. Litkey, H. Kaartinen, J. Hyyppa, E. Ahokas, "Brightness measurements and calibration with airborne and terrestrial laser scanners", Ieee Transactions On Geoscience and Remote Sensing, vol. 46, no. 2, pp. 528-534, 2008, https://doi.org/10.1109/tgrs.2007.911366.
[26] H. Son, C. Kim, N. Hwang, C. Kim, Y. Kang, "Classification of major construction materials in construction environments using ensemble classifiers", Advanced Engineering Informatics, vol. 28, no. 1, pp. 1-10, 2014, https://doi.org/10.1016/j.aei.2013.10.001.
[27] A.R. Smith, "Color gamut transform pairs", ACM Siggraph Computer Graphics, vol. 12, no. 3, pp. 12-19, 1978, https://doi.org/10.1145/800248.807361.
[28] N. Fardin, Q. Feng, O. Stephansson, "Application of a new in situ 3D laser scanner to study the scale effect on the rock joint surface roughness", International Journal of Rock Mechanics and Mining Sciences, vol. 2, no. 41, pp. 329-335, 2004, https://doi.org/10.1016/s1365-1609(03)00111-4.
[29] R.M. Pollyea, J.P. Fairley, "Estimating surface roughness of terrestrial laser scan data using orthogonal distance regression", Geology, vol. 39, no. 7, pp. 623-626, 2011, https://doi.org/10.1130/g32078.1.

[30] FARO, “FARO® LASER SCANNER FOCUS”, Available from: <https://www.faro.com/en-sg/products/construction-bim/faro-laser-scanner-focus/>, Retrieved June 18, 2019.
[31] MathWorks, “MATLAB R2019a”, Available from: <https://www.mathworks.com/products/new_products/latest_features.html?s_tid=hp_release_2019a>, Retrieved June 18, 2019.
[32] FARO, “FARO SCENE”, Available from: <https://www.faro.com/en-gb/products/construction-bim-cim/faro-scene/software/>, Retrieved June 18, 2019.